Effects of Atomic Short-Range Order on the Properties of Perovskite Alloys in their Morphotropic Phase Boundary

A. M. George,[1] Jorge Íñiguez,[2] and L. Bellaiche[1]

[1]*Physics Department, University of Arkansas, Fayetteville, Arkansas 72701, USA*

[2]*Department of Physics and Astronomy, Rutgers University, Piscataway, New Jersey 08854-8019, USA*

(Received 1 April 2003; published 24 July 2003)

The effects of atomic *short-range* order on the properties of $Pb(Zr_{1-x}Ti_x)O_3$ alloy in its morphotropic phase boundary (MPB) are predicted by combining first-principles-based methods and annealing techniques. Clustering is found to lead to a compositional expansion of this boundary, while the association of unlike atoms yields a contraction of this region. Atomic short-range order can thus drastically affect properties of perovskite alloys in their MPB, by inducing phase transitions. Microscopic mechanisms responsible for these effects are revealed and discussed.

DOI: 10.1103/PhysRevLett.91.045504 PACS numbers: 81.30.Bx, 77.22.Ej, 77.80.Bh, 77.84.Dy

Complex insulating perovskite alloys, with the general formula $(A'A''\ldots)(B'B''\ldots)O_3$, are of great interest for a variety of device applications because of their anomalously large electromechanical responses [1–3]. Examples of such applications include piezoelectric transducers and actuators, as well as dielectrics for microelectronics and wireless communication.

Interestingly, many perovskite solid solutions, e.g., $Pb(Zr_{1-x}Ti_x)O_3$ (PZT), $[Pb(Zn_{1/3}Nb_{2/3})O_3]_{1-x}[PbTiO_3]_x$ (PZN–PT), $[Pb(Mg_{1/3}Nb_{2/3})O_3]_{1-x}[PbTiO_3]_x$ (PMN–PT), and $[Pb(Sc_{1/2}Nb_{1/2})O_3]_{1-x}[PbTiO_3]_x$ (PSN–PT), exhibit their largest electromechanical responses for compositions lying within the so-called morphotropic phase boundary (MPB). For more than 50 years this area was thought to *discontinuously* separate, in the temperature-composition plane, a rhombohedral (R) ferroelectric phase exhibiting an electric polarization along a $\langle 111\rangle$ direction from a tetragonal (T) ferroelectric structure having a polarization pointing along a $\langle 001\rangle$ direction. The recent discovery of a monoclinic ferroelectric phase in the MPB of PZT has completely changed this long-accepted picture [4], since this new phase acts as a structural bridge between the R and T phases [4,5]. Furthermore, the polarization in this low-symmetry phase continuously rotates when varying the composition [5,6], explaining why the MPB is the region of choice for optimization of piezoelectric and dielectric responses [5–8]. These recent findings have led to a flurry of investigations aimed at better understanding and characterizing the properties of the MPB in various perovskite alloys. In particular, other low-symmetry phases have also been subsequently discovered in PZN–PT, PMN–PT, and PSN–PT (see, for instance, Refs. [9–15]).

One remaining mystery of the MPB is about its compositional width. More precisely, rather different widths have been reported for the same solid solution, depending on the growth conditions [16]. Chemical short-range ordering (SRO) is often invoked for this variance between different measurements [16], since no long-range ordering occurs (to our knowledge) in the mixed sublattice of PZT and PMN–PT near their MPB. However, why and how SRO would affect the morphotropic phase boundary are two unresolved questions. One possible reason for this lack of knowledge is that the characterization of SRO is challenging and can only be accomplished via nonconventional experiment [17]. Another plausible reason is that mimicking these effects, via the use of computational schemes, requires high accuracy and handling of large supercells, which are two conditions that are not simultaneously met by either usual first-principles techniques or semiempirical approaches.

In this Letter, we take advantage of the accuracy, the possibility of using large supercells, and the microscopic insight provided by the first-principles-based approach of Ref. [5] to study the effect of SRO on the physical properties of PZT in its MPB. The use of this technique (i) proves that SRO does have a drastic effect on these properties, especially in the Ti-poor region of the MPB, (ii) further indicates that short-range association of like atoms has an opposite effect than short-range association of unlike atoms on the compositions delimiting the MPB, and (iii) reveals the microscopic mechanisms responsible for these features.

Short-range ordering in any $A(B'_{1-x}B''_x)O_3$ perovskite alloy can be characterized by the so-called Cowley parameters, defined as [18]

$$\alpha_j(x) = 1 - \frac{P(j)}{x}, \tag{1}$$

where $P(j)$ is the probability of finding a B' (B'') atom being the jth nearest neighbor of a B'' (B') atom in the mixed B sublattice. Then, $\alpha_j(x) = 0$ for all j's represents a *truly disordered alloy* while $\alpha_j(x) > 0$ is associated with clustering, that is jth nearest neighbors are preferentially of the same atomic kind. The converse—a configuration for which $\alpha_j(x) < 0$—corresponds to *anticlustering,* that is, to a situation in which jth nearest neighbors are

preferentially of a different atomic kind. Note that an increase in the magnitude of α_j is indicative of an increase in the strength of SRO. We focus here on relatively small ordering deviations occurring over the first nearest neighbor's shell from the perfectly disordered $Pb(Zr_{1-x}Ti_x)O_3$ alloys. Practically, we limit ourselves to the range $-0.3 < \alpha_1 < 0.3$, while always stipulating that $\alpha_2 = \alpha_3 = 0$. We use a simulated annealing technique [19] that allows us to determine the $12 \times 12 \times 12$ atomic configuration $\{\sigma_i\}$, where $\sigma_i = +1$ or -1 corresponds to the presence of a Zr or Ti atom, respectively, at the B-sublattice site i of PZT, that best satisfies the prefixed Cowley parameters. Once the desired atomic configuration is generated, it is used for input in Monte Carlo simulations utilizing the first-principles-derived alloy effective Hamiltonian proposed in Refs. [5,6]. All the simulations conducted in the present study are done at 50 K. The outputs of the Monte Carlo procedure are the set of polar local soft modes $\{\mathbf{u}_i\}$, where i indexes the different five-atom perovskite cells [20], and the homogeneous strain tensor. The $\langle \mathbf{u} \rangle$ supercell average of the $\{\mathbf{u}_i\}$ modes is directly proportional to the macroscopic electrical polarization. The $\{\mathbf{u}_i\}$ supercell distribution is also used to compute the $f_\mu(\mathbf{k})$ coefficients defined as

$$f_\mu(\mathbf{k}) = \beta \sum_i \exp(i\mathbf{k} \cdot \mathbf{R}_i) u_{i,\mu}, \qquad (2)$$

where $\mathbf{k}$ is a vector in the first Brillouin zone of the simple perovskite structure and $\mathbf{R}_i$ is the lattice vector associated with cell i. μ identifies the Cartesian coordinate (the x, y, and z axes are chosen along the pseudocubic [100], [010], and [001] directions, respectively) of the local modes $\mathbf{u}_i$. β is a normalization coefficient yielding $\sum_k |f_\mu(\mathbf{k})|^2 = 1$. It is important to realize that a value close to 1 for $|f_\mu(\mathbf{k})|^2$ at $\mathbf{k} = 0$, i.e., for the Γ point, corresponds to the homogeneous situation where the μ component of $\mathbf{u}_i$ is nearly independent of the cell i. On the other hand, the inhomogeneous case in which the local polarization fluctuates from its averaged value between different cells yields a $|f_\mu(\mathbf{k})|^2$ that is smaller than 1 for $\mathbf{k} = 0$. The larger this real-space fluctuation is, the smaller $|f_\mu(\mathbf{k})|^2$ at Γ.

Figure 1 shows the composition dependence of the x, y, and z Cartesian coordinates ($\langle u_x \rangle$, $\langle u_y \rangle$, and $\langle u_z \rangle$) of $\langle \mathbf{u} \rangle$ as a function of composition in disordered materials. As indicated in previous studies [5,6], our effective Hamiltonian approach successfully predicts the existence of three ferroelectric phases for random $Pb(Zr_{1-x}Ti_x)O_3$ solid solutions near its MPB: a tetragonal *(T)* phase for $x > 48.7\%$, a rhombohedral *(R)* phase for $x < 47.7\%$, and the recently discovered monoclinic [4], and so-called M_A [24], phase for the composition range $\Delta x = 1.0\%$ in between. The polarization is parallel to the pseudocubic [001], [111], or $[vv1]$ (with $0 < v < 1$) direction for the T, R, and M_A phases, respectively. The electrical polarization can thus be viewed as rotating in a $(\bar{1}10)$ plane from [001] to [111] in the M_A phase as the Ti composition

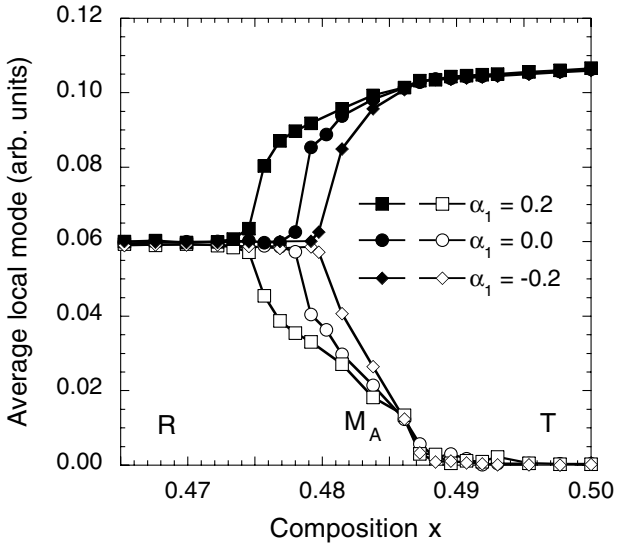

FIG. 1. ($\langle u_x \rangle$, $\langle u_y \rangle$, $\langle u_z \rangle$) Cartesian coordinates of the supercell average of the local mode vectors, as a function of composition in $Pb(Zr_{1-x}Ti_xO_3)$ solid solutions. Circles correspond to disordered alloys (i.e., $\alpha_1 = \alpha_2 = \alpha_3 = 0$), while squares and diamonds correspond to solid solutions exhibiting short-range clustering ($\alpha_1 = +0.2$, and $\alpha_2 = \alpha_3 = 0$) and anticlustering ($\alpha_1 = -0.2$, and $\alpha_2 = \alpha_3 = 0$), respectively. The filled symbols represent the z component, while the open symbols are associated with the x and y components (which are always equal to each other). T, M_A, and R denote the tetragonal, monoclinic, and rhombohedral phases discussed in the text.

decreases [5]. Note that the precise compositions at which the T-to-M_A and M_A-to-R phase transitions occur are numerically found by identifying these compositions with those yielding a peak in the electromechanical responses [6].

Figure 1 also illustrates the effect of short-range clustering and anticlustering on the compositions delimiting the MPB, by displaying $\langle \mathbf{u} \rangle$ as a function of x in $Pb(Zr_{1-x}Ti_x)O_3$ alloys characterized by $\alpha_1 = +0.2$ and $\alpha_1 = -0.2$, respectively. Striking features revealed by Fig. 1 are that SRO clustering considerably widens this morphotropic phase boundary, while SRO anticlustering leads to a significant compositional narrowing of the MPB with respect to the random case. As a matter of fact, samples associated with $\alpha_1 = +0.2$ and $\alpha_1 = -0.2$ exhibit a MPB width of 1.3% and 0.7%, respectively. These are quite remarkable changes with respect to the corresponding width of 1.0% for disordered materials, when recalling that the short-range orders considered here occur only in the first nearest neighbor shells and have a relatively small strength. Interestingly, Fig. 1 shows that the T-M_A transition happens near the same Ti compositions of 48.7%, independently of the value and sign of α_1. It is thus the M_A-R transition point that is shifting to smaller (larger) Ti concentrations with increasing clustering (anticlustering). In other words, SRO has nearly no effect on the direction of the polarization in the Ti-rich area of the MPB of PZT, while it can

considerably affect the properties of the Ti-poor region of this MPB. This drastic difference may be related to the fact that the derivative of $\langle \mathbf{u} \rangle$ with respect to composition has a much smaller magnitude for large Ti compositions than for small Ti concentrations in the MPB of disordered PZT (see Fig. 1). Consequently, the total electrical polarization may be less sensitive to a slight change of atomic configuration (i.e., a slight modification in composition or in SRO) for larger x than for smaller x in the MPB of $Pb(Zr_{1-x}Ti_x)O_3$. The different behavior of the Ti-rich and Ti-poor sides of the MPB may also be related to the fact that the T-M_A transition is second order in character while the M_A-R transition is first order [24]. Identifying the precise microscopic mechanism responsible for the insensitivity of the Ti-rich area of the MPB of PZT with SRO remains for future work.

In light of the results shown in Fig. 1, we decided to investigate in more detail the Ti-poor area of the MPB. Figure 2(a) shows that, as α_1 increases above zero (clustering), the polarization of $Pb(Zr_{0.52}Ti_{0.48})O_3$ tends to rotate within a $(\bar{1}10)$ plane and *toward the [001] direction*, since $\langle u_z \rangle$ becomes larger while $\langle u_x \rangle$ and $\langle u_y \rangle$ are reduced in magnitude. (We find that even for very large values of α_1 that are not shown here, the resulting phase remains monoclinic rather than becoming tetragonal.) This is consistent with the clustering-induced widening of the Ti-poor region of the MPB area displayed in Fig. 1. Figure 2(a) further demonstrates that, as expected by looking at Fig. 1, decreasing α_1 below zero (anticlustering) leads to a rotation of the polarization within a $(\bar{1}10)$ plane and *toward the [111] crystallographic direction.* [In fact, the polarization actually reaches the [111] direction characteristic of the R phase for values of α_1 below -0.2 in $Pb(Zr_{0.52}Ti_{0.48})O_3$.] Figure 2(b) shows the behavior of $|f_\mu(\mathbf{k}=0)|^2$ [see Eq. (2)] versus α_1. Figure 2(c) shows the SRO dependence of the magnitude of $\langle \mathbf{u} \rangle$ as compared to those of $\langle \mathbf{u}_{Zr} \rangle$ and $\langle \mathbf{u}_{Ti} \rangle$, the local-mode averages restricted to cells occupied by Zr and Ti atoms, respectively. Figure 2(d) displays the variation of the angle between the pseudocubic [001] direction and $\langle \mathbf{u} \rangle$, $\langle \mathbf{u}_{Zr} \rangle$, and $\langle \mathbf{u}_{Ti} \rangle$ as a function of α_1. Figure 2(b) reveals that increasing clustering leads to a larger fluctuation of the x and y components of the local polarization associated with the five-atoms-unit cells, as demonstrated by the decrease of $|f_x(\mathbf{k}=0)|^2$ and $|f_y(\mathbf{k}=0)|^2$ as α_1 increases. Figures 2(c) and 2(d) tell us that this large fluctuation is correlated with the clustering-induced enhancement of difference between $\langle \mathbf{u}_{Zr} \rangle$ and $\langle \mathbf{u}_{Ti} \rangle$: for large values of α_1, the local polarizations associated with cells centered on Zr atoms are much closer to the [111] direction, and much smaller in magnitude, as consistent with Refs. [22,23], than the local polarizations associated with cells centered on Ti atoms. In other words, clustering allows the cells centered on Zr and Ti atoms to have rather different ferroelectric properties.

Let us now discuss and understand the results depicted in Fig. 2. Two helpful trends can be formulated by

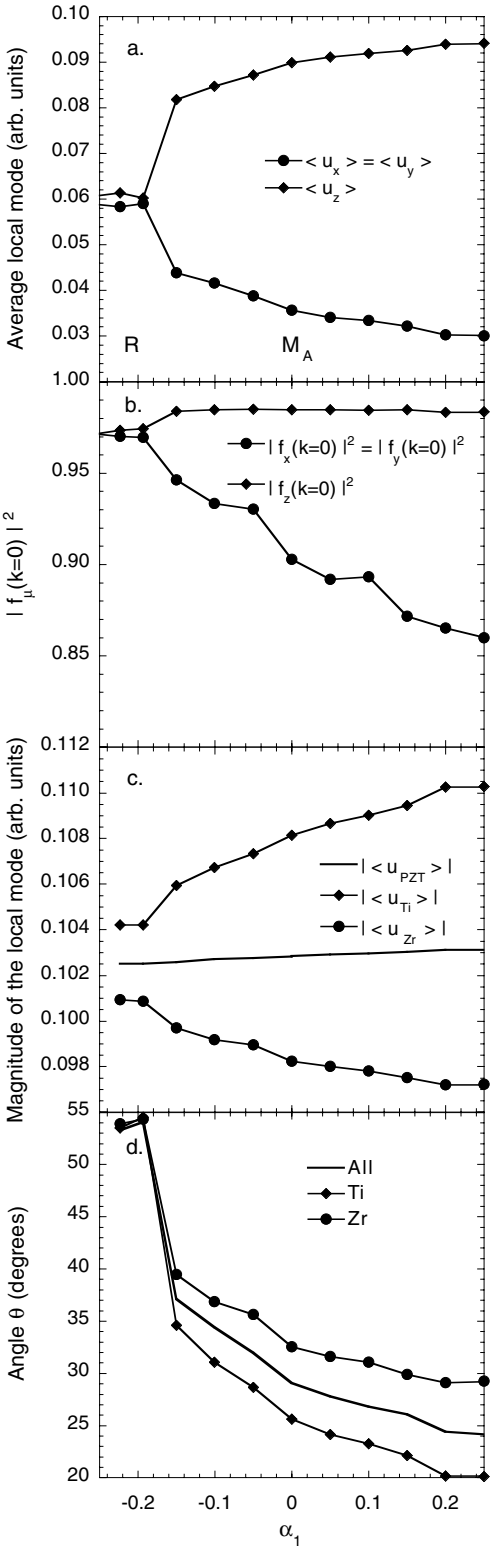

FIG. 2. Properties of $Pb(Zr_{0.52}Ti_{0.48})O_3$ as a function of the α_1 SRO parameter. (a) ($\langle u_x \rangle$, $\langle u_y \rangle$, $\langle u_z \rangle$) Cartesian coordinates of the supercell average of the local mode vectors, (b) Fourier coefficients defined in Eq. (2) and computed at the Γ point, (c) magnitude of the local mode vectors averaged over the five-atom cells centered on Zr (circles), Ti (diamonds), and on all the B atoms (solid line), (d) same as (c) but for the angle between these local modes and the [001] direction.

inspecting the parameters of our alloy effective Hamiltonian for PZT [5,6]. Trend I is that alloy on-site terms favor atomic-induced distinction between local modes, namely, local modes associated with cells occupied by Ti (Zr) atoms want to align along a $\langle 100 \rangle$ tetragonal ($\langle 111 \rangle$ rhombohedral) direction. Trend II is that the intersite interactions between a local-mode $\mathbf{u}_i$ centered on the ith cell and the local modes $\mathbf{u}_j$ associated with its neighbors favor similarity between $\mathbf{u}_i$ and $\mathbf{u}_j$. In other words, an homogeneous distribution of modes is energetically favored by trend II. When clustering of alike atoms occurs, Ti- and Zr-rich regions tend to develop dipole moments aligned along tetragonal and rhombohedral directions, respectively [see Fig. 2(d)], in order to satisfy both trends I and II inside each of these regions. Moreover, trend II ensures that dipole moments of these different regions are correlated, which results in a very homogeneous distribution of $u_{i,z}$ local-mode components and a significantly disordered distribution of $u_{i,x}$ and $u_{i,y}$ [see Fig. 2(b) and note that z is the preferential polarization direction of the Ti-rich regions]. Hence, clustering favors an overall spatially inhomogeneous monoclinic M_A phase in the Ti-poor area of the MPB. On the other hand, anticlustering leads to an incompatibility between trends I and II even at a very short-range scale. As a matter of fact, local modes following their particular trend of being either tetragonal or rhombohedral will find the opposition of their first nearest neighbors already. This results in a more homogeneous local-mode distribution, as shown in Fig. 2. Very importantly, our results prove that this homogeneity leads to the suppression of the monoclinic phase. Indeed, Fig. 2 shows that upon decreasing α_1 we get a distinct transition from an inhomogeneous to a more homogeneous distribution of local modes that is accompanied by a macroscopic monoclinic to rhombohedral phase transition. It is now clear why anticlustering results in a smaller MPB region, as shown in Fig. 1. Our results are consistent with Refs. [23,25], in which it was pointed out that inhomogeneity is essential to the existence of the monoclinic phase.

In summary, we have performed *ab initio*–based simulations to study the effects of SRO, occurring over the first nearest neighbor's shell of the B-mixed sublattice, on the structural properties of PZT near its MPB. A competition between two different energy-induced trends in the Ti-poor area of the MPB leads to a considerable widening of the MPB area when clustering occurs, while yielding a significant narrowing of this phase boundary when anticlustering develops. The electromechanical properties of PZT in the Ti-poor region of its MPB thus drastically depend on the SRO, since they are extremely sensitive to the direction of the polarization [6]. In light of these predictions, we hope that the present Letter will encourage the attempt of experiments aimed at characterizing atomic short-range order in the MPB of perovskite solid solutions. Such experiments are very frequent in metallic alloys [17], but (to our knowledge) have not yet been conducted in ferroelectric alloys.

This work is supported by National Science Foundation Grant No. DMR-9983678 and Office of Naval Research Grants No. N00014-01-1-0365, No. N00014-01-1-0600, and No. N0014-97-1-0048.

[1] K. Uchino, *Piezoelectric Actuators and Ultrasonic Motors* (Kluwer Academic Publishers, Boston, 1996).
[2] S.-E. Park and T. R. Shrout, J. Appl. Phys. **82**, 1804 (1997).
[3] O. Auciello, J. F. Scott, and R. Ramesh, Phys. Today **51**, No. 7, 22 (1998).
[4] B. Noheda *et al.*, Appl. Phys. Lett. **74**, 2059 (1999).
[5] L. Bellaiche, A. García, and D. Vanderbilt, Phys. Rev. Lett. **84**, 5427 (2000).
[6] L. Bellaiche, A. García, and D. Vanderbilt, Ferroelectrics **266**, 41 (2002).
[7] R. Guo *et al.*, Phys. Rev. Lett. **84**, 5423 (2000).
[8] H. Fu and R. E. Cohen, Nature (London) **403**, 281 (2000).
[9] D. E. Cox *et al.*, Appl. Phys. Lett. **79**, 400 (2001).
[10] D. La-Orauttapong *et al.*, Phys. Rev. B **65**, 144101 (2002).
[11] Z.-G. Ye *et al.*, Phys. Rev. B **64**, 184114 (2001).
[12] B. Noheda *et al.*, Phys. Rev. B **66**, 054104 (2002).
[13] J-M. Kiat *et al.*, Phys. Rev. B, **65**, 064106 (2002).
[14] A. K. Singh and D. Pandey, J. Phys. Condens. Matter **13**, L931 (2001).
[15] R. Haumont, B. Dkhil, J.M. Kiat, A. Al-Barakaty, and L. Bellaiche, Phys. Rev. B (to be published).
[16] Ragini, R. Ranjan, S. K. Mishra, and D. Pandey, J. Appl. Phys. **92**, 3266 (2002).
[17] L. Reinhard and S. C. Moss, Ultramicroscopy **52**, 223 (1993).
[18] L. Bellaiche and A. Zunger, Phys. Rev. B **57**, 4425 (1998).
[19] J. Íñiguez and L. Bellaiche, Phys. Rev. Lett. **87**, 095503 (2001).
[20] $\mathbf{u_i}$ is the polar displacement pattern occurring in cell i, centered on a B atom, and related to the ferroelectric soft mode eigenvector of the force constant matrix $(\chi_{\mathrm{Pb}}, \chi_{\mathrm{B}}, \chi_{\mathrm{O}_\parallel}, \chi_{\mathrm{O}_\perp}, \chi_{\mathrm{O}_\perp})$ [21]. For PZT, we numerically find that $(\chi_{\mathrm{Pb}}, \chi_{\mathrm{B}}, \chi_{\mathrm{O}_\parallel}, \chi_{\mathrm{O}_\perp}, \chi_{\mathrm{O}_\perp}) = (0.76, 0.19, -0.18, -0.42, -0.42)$. The large value of χ_{Pb} implies that Pb atoms play an important role on the ferroelectric properties of PZT, as consistent with Refs. [22,23].
[21] W. Zhong, D. Vanderbilt, and K. M. Rabe, Phys. Rev. B **52**, 6301 (1995).
[22] W. Dmowski, T. Egami, L. Farber, and P. K. Davies, in *Fundamental Physics of Ferroelectrics 2001*, edited by H. Krakauer, AIP Conf. Proc. No. 582 (AIP, New York, 2001), p. 33.
[23] I. Grinberg, V. R. Cooper, and A. M. Rappe, Nature (London) **419**, 909 (2002).
[24] D. Vanderbilt and M. H. Cohen, Phys. Rev. B, **63**, 094108 (2001).
[25] A. M. George, J. Íñiguez, and L. Bellaiche, Phys. Rev. B, **65**, R180301 (2002).